Biosensors and Bioelectronics 130 (2019) 166–173

Contents lists available at ScienceDirect

Biosensors and Bioelectronics

journal homepage: www.elsevier.com/locate/bios

Dual-type responsive electrochemical biosensor for the detection of α2,6-sialylated glycans based on AuNRs-SA coupled with c-SWCNHs/S-PtNC nanocomposites signal amplification

Jia Li[1], Junlin He[1], Chengli Zhang, Jun Chen, Weiran Mao, Chao Yu*

College of Pharmacy, Institute of Life Science and School of Public Health, Chongqing Medical University, Chongqing 400016, PR China

ARTICLE INFO

Keywords:
α2,6-sialylated Glycans
Single-walled carbon nanohorns
Sambucus Nigra Agglutinins
Biosensor
Sulfur-doped platinum nanocluster

ABSTRACT

In this study, a dual-type responsive electrochemical biosensor was developed for the quantitative detection of α2,6-sialylated glycans (α2,6-sial-Gs), a potential biomarker of tumors. The gold nanorods (AuNRs), which exhibited great specific surface area, as well as good biocompatibility, was synthesized by the way of seed growth method. Furthermore, a biotin-streptavidin (biotin-SA) system was introduced to improve the immunoreaction efficiency. Accordingly, a label-free biosensor was fabricated based on AuNRs-SA for the quick detection of α2,6-sial-Gs by recording the signal of differential pulse voltammetry (DPV). Furthermore, to expand the ultrasensitive detection of α2,6-sial-Gs, a carboxylated single-walled carbon nanohorns/sulfur-doped platinum nanocluster (c-SWCNHs/S-PtNC) was synthesized for the first time as a novel signal label, which showed an excellent catalytic performance. The usage of c-SWCNHs/S-PtNC could significantly amplify the electrochemical signal recorded by the amperometric i-t curve. Herein, a sandwich type biosensor was constructed by combining the AuNRs-SA on the electrode and c-SWCNHs/S-PtNC (signal amplifier). The label-free biosensor possessed a linear range from 5 ng mL^{-1} to 5 μg mL^{-1} with a detection limit of 0.50 ng mL^{-1}, and the sandwich-type biosensor possessed a wide linear range from 1 fg mL^{-1} to 100 ng mL^{-1} with a detection limit of 0.69 fg mL^{-1}. Furthermore, the biosensor exhibited excellent recovery and stability, indicating its potential for use in actual samples.

1. Introduction

N-acetylneuraminic acid (Neu5Ac), also called sialic acid, acted as terminal monosaccharide by linking with cell surface glycoconjugate (Kim et al., 2011). The formation of α2,6-linkages between sialic acid and N-acetyllactosamine structures (Galβ1–4GlcNAc) is mediated by the enzyme β-galactoside α2,6-sialyltransferase (ST6Gal-I) (Harduin-Lepers et al., 2001). In recent reports, a wide number of biological and pathological disorders have been found to display variants of a α2,6-sialylation, such as the development and progression of colon and liver cancer (Dall'Olio et al., 1989; Schultz et al., 2013; Zhao et al., 2017). While the carcinoma cells were apoptotic, the α2,6-sialylated glycans (α2,6-sial-Gs) were formed and released into the blood, adding to an increased concentration of α2,6-sial-Gs in human serum. Moreover, high concentrations of α2,6-sial-Gs have been detected in colon and liver cancer (Gessner et al., 1993), suggesting that α2,6-sial-Gs could be used as clinical cancer biomarker.

Until recently, there were a few methods for detecting sialylated glycans, such as electrospray mass spectrometry (Saarinen et al., 1999), high-performance liquid chromatography-mass spectrometry (Harvey, 2011), and miniaturized glycosyltransferase assays (Patil et al., 2014). However, these methods require professional technicians, long analysis time and high-cost, which limit their widespread use. Therefore, earlier attempts have explored novel detection techniques for the sensitive analysis of sialylated glycans. In recent years, sandwich-type biosensors have received attention as one of the important analytical techniques for the sensitive and specific detection of proteins (Gevaerd et al., 2018; Li et al., 2016a, 2016b; Lima et al., 2018). However, the use of this design to detect glycans was limited in biomedical applications due to the absence of a second specific antibody. In this research, a novel recognition system to detect α2,6-sial-Gs was fabricated with specific a recognition component for Sambucus nigra agglutinins (SNA) (Li et al., 2015; Park et al., 2012) and a nonspecific recognition component for 3-aminophenylboronic acid (M-APBA) (Otsuka et al., 2003). We

* Correspondence to: College of Pharmacy, Chongqing Medical University, Box 380#, 1 Yi Xue Yuan Road, Chongqing 400016, PR China.
E-mail address: yuchaom@163.com (C. Yu).
[1] Junlin He and Jia Li contributed equally to this work.

https://doi.org/10.1016/j.bios.2019.01.054
Received 30 November 2018; Received in revised form 19 January 2019; Accepted 22 January 2019
Available online 01 February 2019
0956-5663/

successfully constructed a sandwich electrochemical biosensor and combined it with a label-free electrochemical biosensor to construct a novel dual-type responsive electrochemical biosensor. The novel biosensor performed wider detection range than the conventional electrochemical biosensors (Zhang et al., 2018a, 2018b, 2018c, 2018d).

In recent years, gold nanomaterials have been widely applied to the field of biosensors due to their excellent electrical conductivity and biocompatibility, and studies on nanomaterials have found that gold nanomaterials can form different morphologies, such as nanoparticles and nanorods (Narang et al., 2015; Skrabalak et al., 2007; Won et al., 2011; Yavas et al., 2018). Compared with gold nanoparticles, gold nanorods (AuNRs) have greater specific surface area and better biocompatibility (Narang et al., 2015). Thus, AuNRs can be used as better carriers to bind SNA. To improve the sensitivity (positively correlated to the numbers of SNA) of the proposed biosensor, biotinylated Sambucus nigra (Elderberry) bark lectin (bio-SNA) was used instead of SNA to build the biotin-streptavidin system (Wu et al., 2017). Streptavidin (SA) were used to immobilize the surface of the AuNRs; subsequently, bio-SNA could load on the electrode in a large amount. Based on this sequential administration mode, a label-free biosensor was fabricated using AuNRs-SA as the support platform, which can conduct the quick detection of α2,6-sial-Gs via the differential pulse voltammetry (DPV) method (Zhang et al., 2018a, 2018b, 2018c, 2018d).

Therefore, to achieve higher sensitivity in the detection of α2,6-sial-Gs, a sandwich-type biosensor was introduced. The crucial factor in developing a sandwich-type biosensor was substrate material (AuNRs-SA) cooperating with the signal materials to achieve a sufficient signal amplification. Thus, the choice of signal material was particularly important (Wang et al., 2015). Due to the excellent catalytic properties of some nanomaterials, more attentions have been placed on the application of nanomaterials for biosensors to achieve signal amplification. Specifically, platinum (Pt) based nanostructures have been revealed to conduct outstanding electrocatalytic activity with hydrogen peroxide (H_2O_2), which is of immense importance for electrochemical energy conversion (Sanzò et al., 2017). Furthermore, sulfur-doped metals exhibit remarkable physical and chemical properties, and are appropriate for a diverse range of applications (Bemana and Rashid-Nadimi, 2017). To our knowledge, sulfur-doped Pt has not been exploited for electrochemical detections. Herein, a sulfur-doped Pt nanocluster (S-PtNC) was successfully synthesized, and displayed good catalytic property as well as numerous absorption/active sites, which indicates that S-PtNC is a suitable signal material. To further achieve the signal amplification, single-walled carbon nanohorns (SWCNHs) were applied to fix S-PtNC on the surface, as a novel nanomaterial with good conductivity, a large specific surface area and low toxicity (Dong et al., 2012; Liu et al., 2017). The usage of SWCNHs increased the amount of S-PtNC fixed on the surface of the SWCNHs and promoted the electrochemical signal through the cocatalytic effect. To improve the biocompatibility of SWCNHs, Yang's group synthesized carboxylated SWCNHs (Yang et al., 2014). And the further grafted with M-APBA through Pt-NH_2 bond and -CO-NH- bond, the biocompatible carboxylated SWCNHs-S-PtNC (c-SWCNHs/S-PtNC) could achieve signal amplification for offering more combination sites. Therefore, a novel sandwich-type biosensor was designed using a AuNRs-SA as the sensing matrix and c-SWCNHs/S-PtNC as the signal label via the amperometric i-t curve method.

In this work, a label-free electrochemical biosensor was designed using AuNRs-SA as the support platform to achieve the quick detection of α2,6-sial-Gs. The AuNRs-SA and bio-SNA were modified on the surface of a glassy carbon electrode (GCE), forming a sensing interface with the α2,6-sial-Gs. With the increasing α2,6-sial-Gs concentration, the DPV current response decreased. Further, to realize the ultrasensitive detection of α2,6-sial-Gs, c-SWCNHs/S-PtNC was introduced as the signal tag. Combining with AuNRs-SA, a novel sandwich-type biosensor was fabricated (Scheme 1). In the presence of the target, c-SWCNHs/S-PtNC/M-APBA could be immobilized on the fabricated biosensor. As a result, an increased current response was recorded in a phosphate buffered saline (PBS) solution through the addition of 20 μL of H_2O_2. This dual-type responsive electrochemical biosensor has three major advantages: 1) The label-free biosensor provides a quick analysis of α2,6-sial-Gs and may be a feasible alternative for point-of-care testing. 2) The sandwich-type biosensor provides an ultrasensitive detection of α2,6-sial-Gs and has great potential for detecting the low level of biomarker. Moreover, the dual-type responsive biosensor could also be combined to increase the detection range and potential of practical application. 3) Compared with individual SWCNHs and S-PtNC, c-SWCNHs/S-PtNC composites have a more efficient catalytic ability.

2. Experimental

2.1. Materials and reagents

Neu5Ac α(2−3)Gal β MP glycoside and Neu5Ac α(2−6)Gal β MP glycoside were provided by Tokyo Chemical Industry. Biotinylated Sambucus nigra (Elderberry) bark lectin (bio-SNA) was purchased from Vector Laboratories, Inc. (USA, Burlingame, www.vectorlabs.com). Potassium tetrachloroplatinate (I) (K_2PtCl_4) was purchased from MACKLIN (Shanghai, China). Methylene blue (MB), bovine serum albumin (BSA, 96–99%), streptavidin (SA), N-hydroxy succinimide (NHS) N-(3-dimethylaminopropyl)-N′-ethylcarbodiimidehydrochloride (EDC) were acquired from Sigma-Aldrich (St. Louis, USA, www.sigmaadrich.com). Gold (III) chloride trihydrate ($HAuCl_4{\cdot}4H_2O$), Hexadecyl trimethyl ammonium bromide (CTAB), silver nitrate ($AgNO_3$), 3-aminophenylboronic acid (M-APBA), Dopamine (DA), L-cysteine, and ascorbic acid (AA) and glucose were purchased from Aladdin (Shanghai, China, www.aladdin-e.com). Single wall carbon nanohorns were purchased from the Nanjing XFNANO Materials Tech Co., Ltd. (Nanjing, China). A phosphate-buffered solution (PBS) was prepared with KH_2PO_4 and Na_2HPO_4 containing 0.15 M NaCl (pH = 7.0). All aqueous solutions used ultrapure grade water afforded by a Millipore Milli-Q system (> 18.2 MΩ cm, USA, www.millipore.com). Potassium ferricyanide ($K_3Fe(CN)_6$) and potassium ferrocyanide ($K_4Fe(CN)_6$) were provided by Beijing Chemical Reagents Company (Beijing, China).

2.2. Apparatus and measurements

All electrochemical experiments, including the amperometric i-t curve, cyclic voltammetry (CV), electrochemical impedance spectroscopic (EIS) and differential pulse voltammetry (DPV) were performed with a CHI 660E workstation (Chenhua Instruments Co., Shanghai, China) at room temperature with a three-electrode system, consisting of a platinum wire electrode as the counter electrode, a saturated calomel electrode (SCE) as the reference electrode and a modified glassy carbon electrode (GCE, 4 mm in diameter) as the working electrode. The morphologies of the different nanomaterials were characterized by transmission electron microscopy (TEM) and field emission scanning electron microscopy (FE-SEM). TEM images were obtained from a Hitachi-7500 (Hitachi Limited, Japan). FE-SEM and energy dispersive X-ray spectroscopy (EDS) images were collected using a JEOL JSM-6700F (Japan, https://www.jeol.co.jp.) and an Oxford x-max50 microscope. X-ray photoelectron spectroscopy (XPS) measurements were performed with a VG Scientific ESCALAB 250 spectrometer (Thermo Nicolet 250XI, USA). Fourier transform infrared (FT-IR) spectrum was recorded by a Nicolet 6700 FT-IR spectrometer (Thermo Nicolet, USA). UV–vis absorption spectra were obtained from a UV-2450 spectrophotometer (Shimazu, Japan). Atomic force microscope (AFM) images were recorded by a Bruker Dimension Icon microscope (USA).

2.3. Preparation of the AuNRs-SA composites

First, the AuNRs were synthesized via a seed growth methodology (Won et al., 2011). To generate the Au seeds, 2.5 mL of a $HAuCl_4$

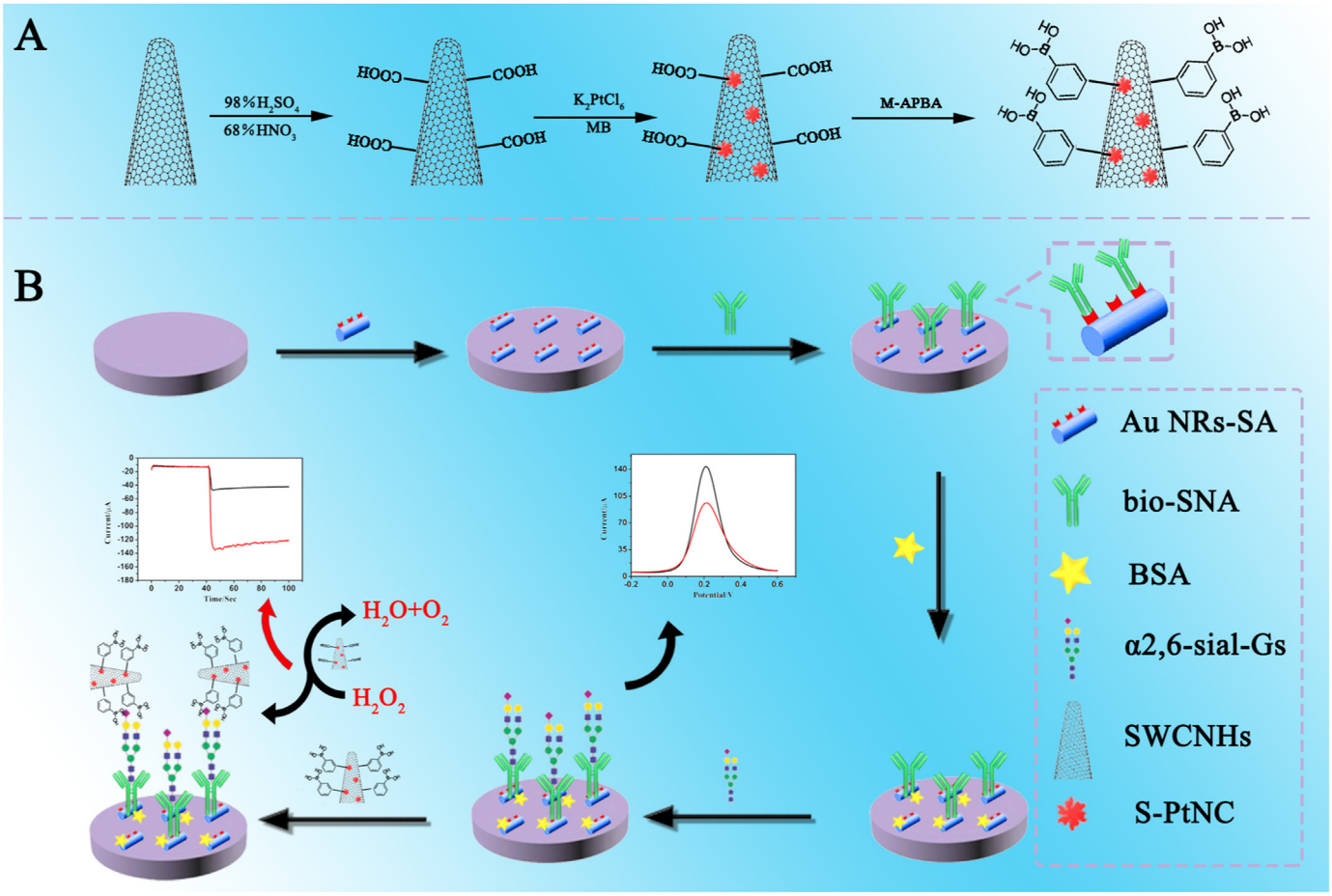

Scheme 1. (A) Preparation process of c-SWCNHs/S-PtNC/M-APBA. (B) Schematic representation of the proposed strategy for the biosensor.

solution (0.5 mM) was mixed with 2.5 mL of a CTAB solution (0.2 mM); next, 300 mL of $NaBH_4$ (0.01 mM) was added and quickly mixed for 2 min, then kept at 25 °C. Then, 5 mL of the $HAuCl_4$ solution (0.2 M) was added to 5 mL of the CTAB solution (1 mM). Next, 0.15 mL of $AgNO_3$ (4 mM) was added to the solution and reacted for 5 min. Then, 70 µL of AA (0.079 mM) was added, and the solution was reacted for 2 min. Then, 12 mL of the prepared Au seed was added to the solution and stirred violently for 20 s and left to react at 25 °C for 2 h. Later, the AuNRs were collected by centrifugation at 5000 rpms for 30 min, washed three times and dissolved in 200 µL of ultrapure water. Then, 40 µL of SA (1 mg mL^{-1}) was added to the solution and shaken overnight. Finally, after washing 3 times, a solution of AuNRs-SA composites were obtained.

2.4. Preparation of c-SWCNHs/S-PtNC composites

The preparation of c-SWCNHs was achieved according to a previously reported procedure (Yang et al., 2014). Initially, SWCNHs were dissolved in a mixed solution of 98% H_2SO_4, 68% HNO_3 and ultrapure water (1:3:6 in volume ratio) and then sonicated for 1 h. Then, the mixture was heated at 40 °C for 6 h to generate the c-SWCNHs. The mixture was centrifuged at 8000 rpm min^{-1} for 5 min and washed three times. Finally, the precipitate was dissolved in 4 mL of ultrapure water prior to use.

A previously reported method was used for the preparation of the c-SWCNHs/S-PtNC, with little modification (Nandan and Nanda, 2013). First, 1 mL of c-SWCNHs (2.5 mg mL^{-1}) solution was sonicated for 5 min. Next, a 5 mL solution of K_2PtCl_4 was prepared by dissolving K_2PtCl_4 powder in ultrapure water, and a 6 mL MB solution (0.1 mM) was prepared. The prepared c-SWCNHs, K_2PtCl_4 and MB solutions were mixed together and heated at 90 °C for 5 h. Finally, the mixture was centrifuged at 10,000 rpm min^{-1} for 5 min, washed three times and dissolved in 1 mL of ultrapure water.

2.5. Preparation of c-SWCNHs/S-PtNC/M-APBA composites

First, 1 mL of the c-SWCNHs/S-PtNC composites, 50 µL of EDC (50 mg mL^{-1}) and 50 µL of NHS (50 mg mL^{-1}) were lightly mixed for 30 min at 4 °C. Next, 50 µL of M-APBA (50 mg mL^{-1}) was added to the compound mixture and stirring continued for 4 h. Then, 100 µL of a 0.25 wt% BSA solution was added to the mixture and lightly mixed for 1 h at 4 °C. Finally, the black precipitates were collected and washed with ultrapure water several times and dispersed in 0.5 mL of ultrapure water.

2.6. Interface modification of the biosensor

A schematic diagram showing the fabrication of the biosensor is presented in Scheme 1. First, the GCE was cleaned by polishing it with 0.3 and 0.05 µm of alumina paste and rinsed with ultrapure water and ethanol. Then, 1.2 mg mL^{-1} of the as-prepared AuNRs-SA composites solution was modified onto the GCE surface and air-dried at room temperature. The attachment of bio-SNA to the modified electrode was achieved by incubating the electrode in an 8 µL solution of bio-SNA (0.2 mg mL^{-1}) for 1.5 h. The electrode was then rinsed with ultrapure water. Next, 6 µL of a 0.25 wt% BSA solution was placed onto the modified electrode in order to block nonspecific sites.

2.7. Electrochemical detection of label-free type and sandwich-type

According to the label-free biosensor detection procedure (Wang et al., 2018), the modified electrode was incubated in different concentrations of standard α2,6-sial-Gs solutions for 2.5 h at 30 °C and then washed with ultrapure water. The DPV was carried out from −0.2 to 0.6 V to record current signals. Furthermore, on the basis of the sandwich-type biosensor detection procedure, 10 μL of the pretreated c-SWCNHs/S-PtNC/M-APBA composites were placed onto the modified electrode and incubated for 2 h at 30 °C. The electrochemical detection signal of the amperometric i-t curve was recorded at −0.4 V in 5 mL of PBS, (pH 7.0) at 25 °C. Until the background current was stable, 20 μL of H_2O_2 (2.0 mol L^{-1}) was added to the PBS solution·H_2O_2 could be catalyzed to H_2O and O_2 by c-SWCNHs/S-PtNC, and an electrical signal was generated, due to the transfer of electrons during the redox process (Fig. S4).

3. Results and discussion

3.1. Characterization of materials

3.1.1. Characterization of AuNR and AuNRs-SA

FE-SEM, TEM, UV–vis, FTIR, EDS and XPS were used to characterize the as-prepared materials. TEM investigated the morphology and structure of the materials. Fig. 1A shows the TEM image of the AuNRs, which had a rod structure with a diameter of 50 nm. When the SA were immobilized on the surface of the AuNRs, the formation of the AuNRs-SA composites by UV–vis spectra and ζ-potential were displayed. As shown in Fig. S6, a salient peak was observed at 710 nm, which belongs to AuNRs. Comparing the UV–vis spectrum of the AuNRs with that of the AuNRs-SA, the AuNRs-SA has a peak at 260 nm due to the SA. Moreover, the ζ-potentials of the AuNRs-SA and Au are illustrated in Fig. S7A; the ζ-potentials of AuNRs and AuNRs-SA were 22.4 and 2.7, respectively. These results indicate that the AuNRs successfully combine with the negatively charged SA (Zhang et al., 2018a, 2018b, 2018c, 2018d).

3.1.2. Characterization of c-SWCNHs/S-PtNC/M-APBA

To demonstrate the successful formation of the signal materials, TEM and FE-SEM were used. The FE-SEM image showed the framework of c-SWCNHs which was stacked by many spherical nanostructures with diameter of approximately 50 ± 10 nm (Fig. 1B). As shown in Fig. S1A, the S-PtNC nanocomposites were dendritic structures with a length of 60 nm. Fig. 1C displays the FE-SEM image of the S-PtNC nanocomposites that were evenly distributed on the surface of the c-SWCNHs. The TEM image (Fig. 1D) illustrates that the S-PtNC nanocomposites were efficiently and successfully attached to the c-SWCNHs. Furthermore, the Pt and S elements were displayed in the EDS of c-SWCNHs/S-PtNC (Fig. 1E), which further demonstrated that the S-PtNC nanocomposite was attached to the surface of the c-SWCNHs. Moreover, the XPS result of the c-SWCNHs/S-PtNC is shown in Fig. 1F and Fig. S5. The XPS results of S-PtNC/c-SWCNHs show signals for C1s at 284.98 eV, for S2p at 164.23 eV, and for Pt4f at 71.28 eV. The XPS reveals that the c-SWCNHs/S-PtNC was successfully synthesized. The ζ-potentials of c-SWCNHs/S-PtNC and c-SWCNHs/S-PtNC/M-APBA were −10.3 and 0.01 (Fig. S7B). These results demonstrated successful modification of the c-SWCNHs/S-PtNC by the positively charged M-APBA. In summary, the signal materials were successfully synthesized. Additionally, we compared the electrochemical behaviors of the different nanomaterials by the amperometric i-t curve in the Supplementary Information (Fig. S1B).

3.2. Characterization of the proposed biosensor

First, we used an electrochemical impedance spectroscopy (EIS) measurement in a 5 mM $[Fe(CN)_6]^{3-/4-}$ solution to monitor the fabrication procedures of the sensing interface. In the Nyquist diagram, there were two parts: one was a semicircle, and the other one was a line. The semicircle diameter at higher frequencies showed the electron transfer resistance, the linear part at lower frequencies showed the diffusion process (Yuan et al., 2018). As shown in Fig. 2A, the bare GCE presented a small semicircle at high frequency (curve a). After the electrode surface was modified with AuNRs-SA, the resistance was

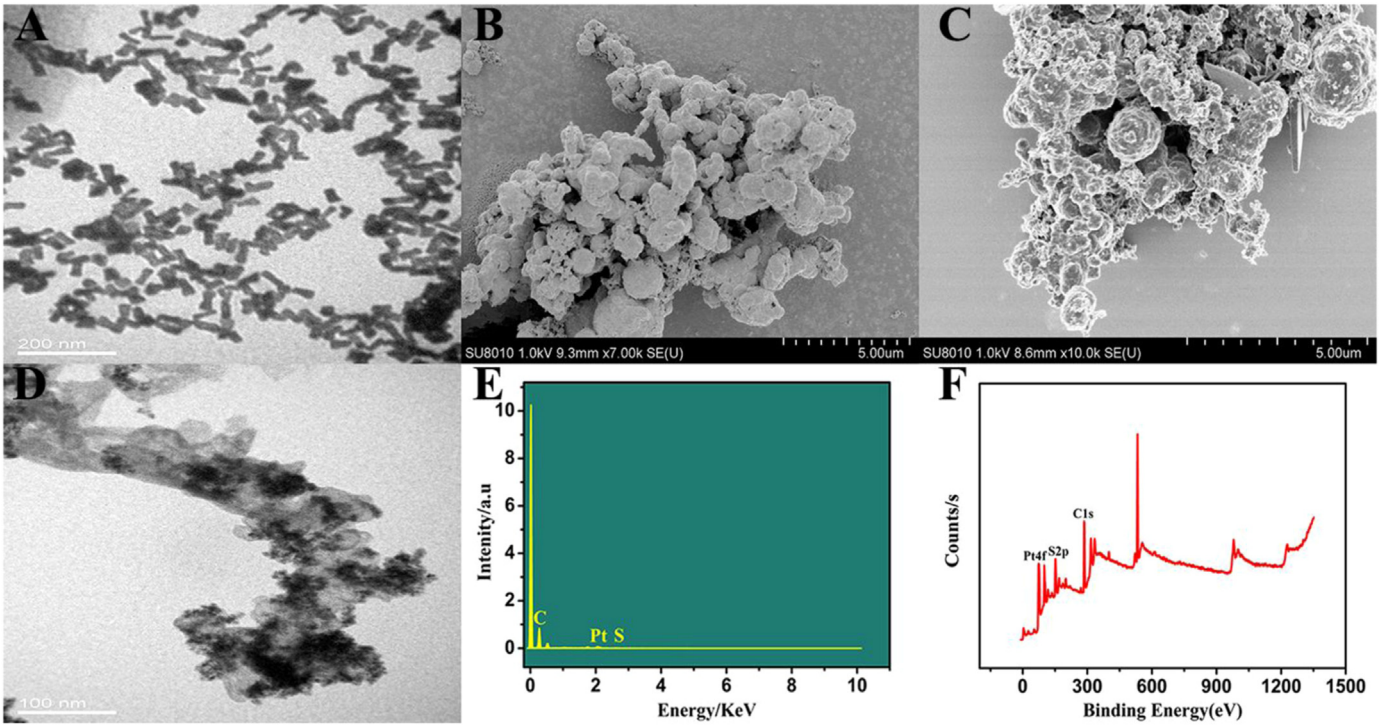

Fig. 1. TEM image of AuNRs (A), FE-SEM images of c-SWCNHs (B), c-SWCNHs/S-PtNC (C). TEM image of c-SWCNHs/S-PtNC (D). EDS image of c-SWCNHs/S-PtNC (E). The XPS spectra of c-SWCNHs/S-PtNC (F).

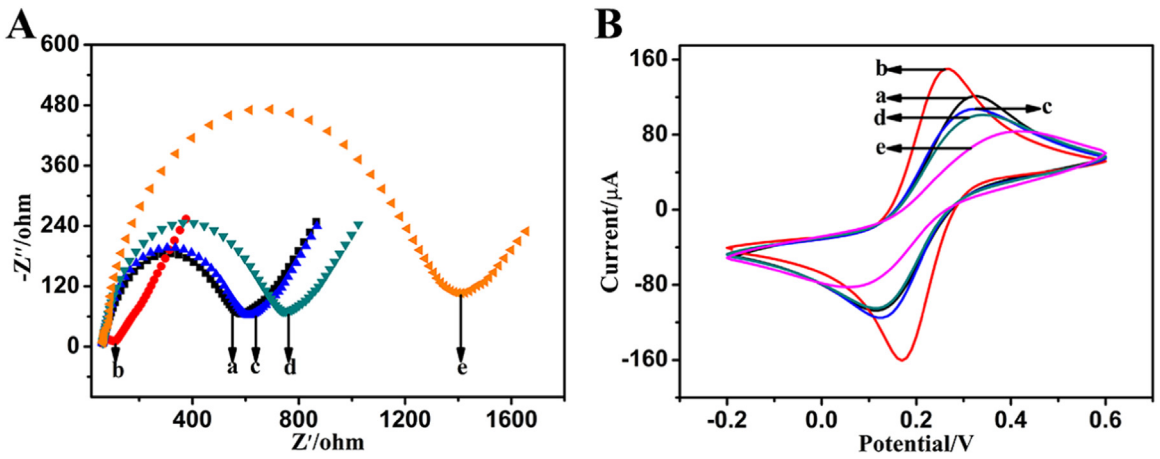

Fig. 2. EIS (A) and CV (B) characterization of the electrodes at various stages of modification in a 5 mM $[Fe(CN)_6]^{3-/4-}$ solution: (a) bare GCE, (b) GCE/AuNRs-SA, (c) GCE/AuNRs-SA/bio-SNA, (d) GCE/AuNRs-SA/bio-SNA/BSA and (e) GCE/AuNRs-SA/bio-SNA/BSA/α2,6-sial-Gs.

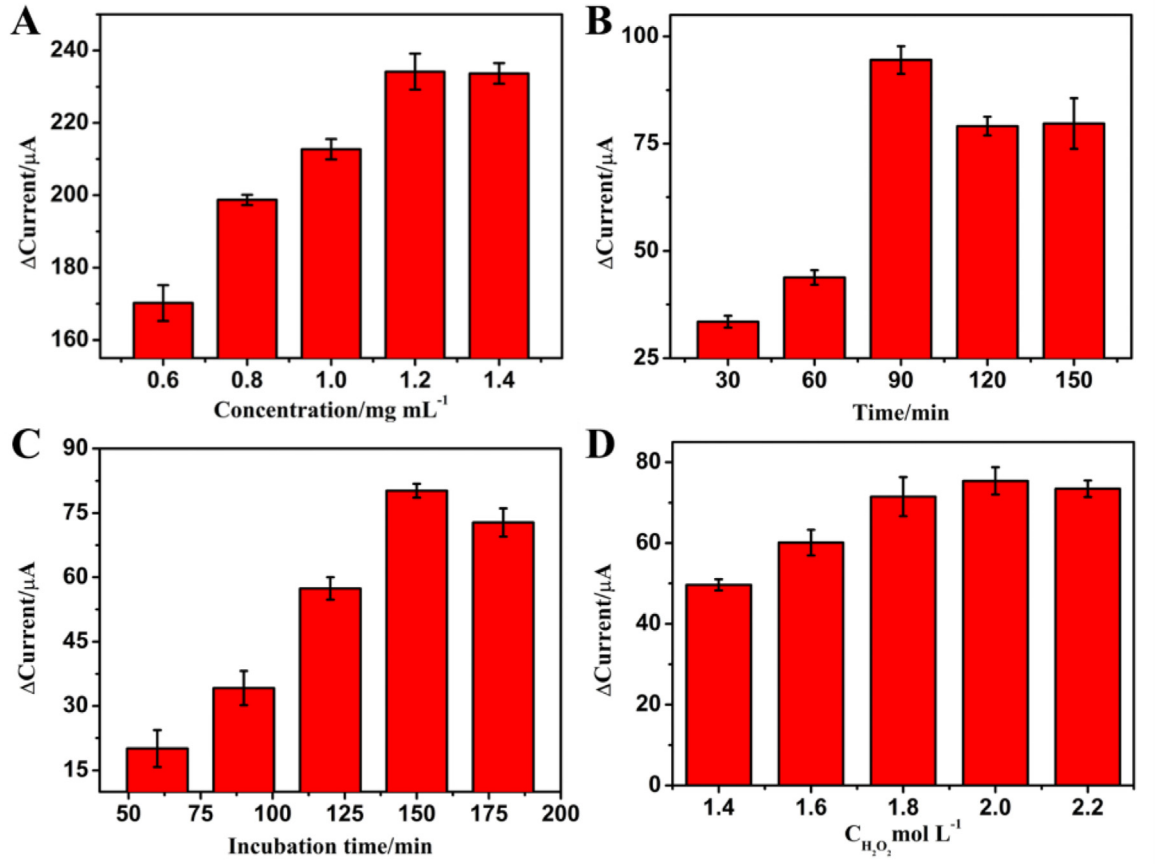

Fig. 3. The effects of the (A) concentration of AuNRs-SA, (B) immobilization time of bio-SNA, (C) incubation time and (D) concentration of H_2O_2.

much less than that of the bare GCE (curve b). This result demonstrated that the AuNRs-SA has excellent conductivity, which can enhance electronic transfer between the electrolyte solution and the electrode surface. After incubating with bio-SNA (curve c), the resistance increased. This result represents that the bio-SNA is fixed on the electrode surface through the specific binding of SA and biotin. Then the resistance further increased (curve d) after the prepared biosensor was blocked with BSA, because BSA hindered the electron transfer. Afterwards, the resistance of curve e further increased due to the α2,6-sial-Gs blocking the electron transfer, therefore demonstrating that the capture of α2,6-sial-Gs was successful.

Cyclic voltammetry (CV) measurements were conducted in a 5 mM $[Fe(CN)_6]^{3-/4-}$ solution to further monitor the fabrication procedures of the sensing interface (Fig. 2B). The bare GCE displayed a couple of typical reversible redox peaks (curve a). After the electrode was coated with AuNRs-SA, the peak current was significantly enhanced (curve b) due to the excellent conductivity of AuNRs-SA. While the bio-SNA was fixed on the modified electrode, the peak current was decreased (curve c) due to the poor conductivity of bio-SNA. After blocking with BSA, the peak current further dropped (curve d) because the BSA hindered the electron transfer. Afterwards, curve e was decreased again displaying that the electron transfer was blocked and the successful capture of α2,6-sial-Gs. These results demonstrate that the fabrication of the biosensor was successful.

In order to demonstrate the successful fabrication of the biosensor, AFM was used to characterize the electrode. As shown in Fig. S8, after the bio-SNA solution was coated onto the AuNRs-SA (Fig. S8B), the surface became smooth compared to the AuNRs-SA modified electrode (Fig. S8A). The mean roughness depth (Rz) of the modified electrode was 18.912 nm. The height of the modified electrode material changed from 9.42 nm to 10.99 nm (Li et al., 2016a, 2016b). Then, BSA was used to block the electrode and the surface smoothness increased slightly. The mean roughness depth (Rz) was measured at 14.107 nm and the height increased to 14.69 nm (Fig. S8C). After α2,6-sial-Gs were coated onto the electrode, the surface became smoother, the mean roughness depth (Rz) was 11.030 nm and the height increased to 16.40 nm due to α2,6-sial-Gs covered the gaps in the electrode surface (Fig. S8D). Collectively, the results illustrate the successful fabrication of the biosensor.

3.3. Optimization of experimental condition

To obtain the optimal electrochemical performance, we investigated factors that may affect biosensor performance, such as the concentration of the AuNRs-SA, the incubation time of the bio-SNA, the incubation time of α2,6-sial-Gs, and the concentration of H_2O_2.

The concentration of AuNRs-SA was investigated to improve the sensitivity of the biosensor and provide a favorable platform for loading the bio-SNA. The concentration of the AuNRs-SA was tested in the range of 0.6 mg mL^{-1} to 1.4 mg mL^{-1}. The results in Fig. 3A show that the changes increased until a concentration of 1.2 mg mL^{-1} and then began to level off. Hence, the optimal concentration of the AuNRs-SA was determined to be 1.2 mg mL^{-1}.

The incubation time of the bio-SNA also played a key role in influencing the performance of the biosensor by dictating the amount of bio-SNA fixed on the electrode surface. The results shown in Fig. 3B indicate that the current change increased with the incubation time from 30 to 90 min and reached the maximum value at 90 min. Therefore, the immobilization of bio-SNA reached saturation at 90 min. Hence, 90 min was considered as the optimal incubation time.

The incubation time of α2,6-sial-Gs is an extremely important factor. From Fig. 3C, we observed that the current change increased from 1.0 to 2.5 h. When the incubation time was longer than 2.5 h, the current remained stable. Therefore, 2.5 h was selected as the optimal incubation time.

In addition, the concentration of H_2O_2 was a critical parameter for the performance of the biosensor. It was found that the current increased with an increase in the concentration of H_2O_2 from 1.4 mol L^{-1} to 2.0 mol L^{-1}. The current remained steady after more than 2.0 mol L^{-1} (Fig. 3D). Hence, the H_2O_2 concentration of 2.0 mol L^{-1} was the optimal condition.

In general, the biosensor performance was best only when the concentration of AuNRs-SA was 1.2 mg mL^{-1}, the incubation time of bio-SNA was 90 min, the incubation time of α2,6-sial-Gs was 2.5 h, and the concentration of H_2O_2 was 2.0 mol L^{-1}.

3.4. Analysis and detection

To explore the performance of the prepared label-free biosensor, a series of α2,6-sial-Gs were detected under the optimal conditions (Fig. 4A). The current signal of the proposed biosensor increased with the increase in α2,6-sial-Gs concentration. This result indicates that the change of the current response was linked to the quantity of glycoside captured. The calibration plot (Fig. 4B) showed a good linear relationship in the range of 5 ng mL^{-1} to 5 μg mL^{-1}, with the limit of detection reaching 0.50 ng mL^{-1} (defined as $DL = 3S_B/m$, where m is the slope of the corresponding calibration curve and S_B is the standard deviation of the blank). The linear regression equation was Y = 12.51 *logC-1.97, with a correlation coefficient of 0.9967. The label-free biosensor achieved the quick and quantitative detection of α2,6-sial-Gs. Then, we explored the performance of the sandwich-type biosensor. The amperometric i-t curves were recorded in 5 mL of PBS (0.1 M, pH 7.0) with 20 μL of H_2O_2 added to the solution. The current response was shown in Fig. 4C. The current increased gradually with increase in concentration from 10 fg mL^{-1} to 100 ng mL^{-1}. As shown in Fig. 4D, the current response and the logarithm of the α2,6-sial-Gs concentration exhibited a good linear relationship. The linear regression equation was Y = 10.12 *logC + 45.48, with a correlation coefficient of 0.9995. The limit of detection was 0.69 fg mL^{-1}. In comparison with the label-free biosensor, the sandwich-type biosensor had a higher sensitivity and a lower detection limit due to the introduction of c-SWCNHs/S-PtNC/M-APBA. c-SWCNHs/S-PtNC/M-APBA as the signal label had the function of amplifying electrical signals. By combining the label-free biosensor and the sandwich-type biosensor, the detection range can be increased and the biosensor is more practical. Compared with those of a previously reported biosensor for α2,6-sial-Gs in Table 1, the dual-type responsive biosensor achieved much better performance with a wider detection range and a lower detection limit.

3.5. Specificity, stability and reproducibility of the electrochemical biosensor

To evaluate the specificity of the sandwich-type electrochemical biosensor, we compared the effects of some interfering substances, such as Neu5Ac α(2 − 3)Gal β MP glycoside (α2,3-sial-Gs) (1 ng mL^{-1}), AA (1 ng mL^{-1}), glucose (1 ng mL^{-1}), and L-cysteine (1 ng mL^{-1}). The current value of the target α2,6-sial-Gs was significantly higher than that caused by other interferents (Fig. 5A). These experiments confirmed that the current response comes from specific recognition of α2,6-sial-Gs and bio-SNA. These results show the high specificity of the sandwich-type biosensor. The label-free also exhibited excellent specificity in Fig. S3A. The detailed descriptions were shown in the Supplementary information.

Stability is an important factor for evaluating the performance of a biosensor. A series of biosensors were fabricated and stored at 4 °C. After 28 days, the current value of these biosensors remained at 89.63% of the initial current value. The results suggest that the sandwich-type electrochemical biosensor possessed good stability. The reproducibility of the sandwich-type biosensor was evaluated by the measurement of the same concentration of α2,6-sial-G (10 pg mL^{-1}) using five different electrodes (Fig. 5B). The relative standard deviation (RSD) of the biosensor was 0.4796%. It was suggested the sandwich-type biosensor had good precision and reproducibility. In addition, the label-free also exhibited good reproducibility (Fig. S3B).

3.6. Analysis of serum simple

To examine the potentiality of the biosensor for α2,6-sial-Gs analysis in real samples, standard addition method was applied (Ribeiro et al., 2018; Zhang et al., 2018a, 2018b, 2018c, 2018d). The biosensor was applied to analyze the healthy human diluted serum samples spiked with different concentrations of α2,6-sial-Gs. The recovery rates were 96.736–103.41% as shown in Table S1, and the RSDs were less than 5%. The recovery test showed that the biosensor could detect different concentrations of α2,6-sial-Gs in the serum sample, and suggested that the feasibility of the proposed biosensor for clinical application.

4. Conclusion

In summary, a specific dual-type responsive electrochemical biosensor, was fabricated to detect α2,6-sial-Gs. The biosensor uses AuNRs-SA as the sensing platform, which could accelerate the electron transfer rate and load more bio-SNA. As a result, a label-free responsive electrochemical biosensor was achieved. And c-SWCNHs/S-PtNC as the novel signal label, was used to fabricate the sandwich-type biosensor,

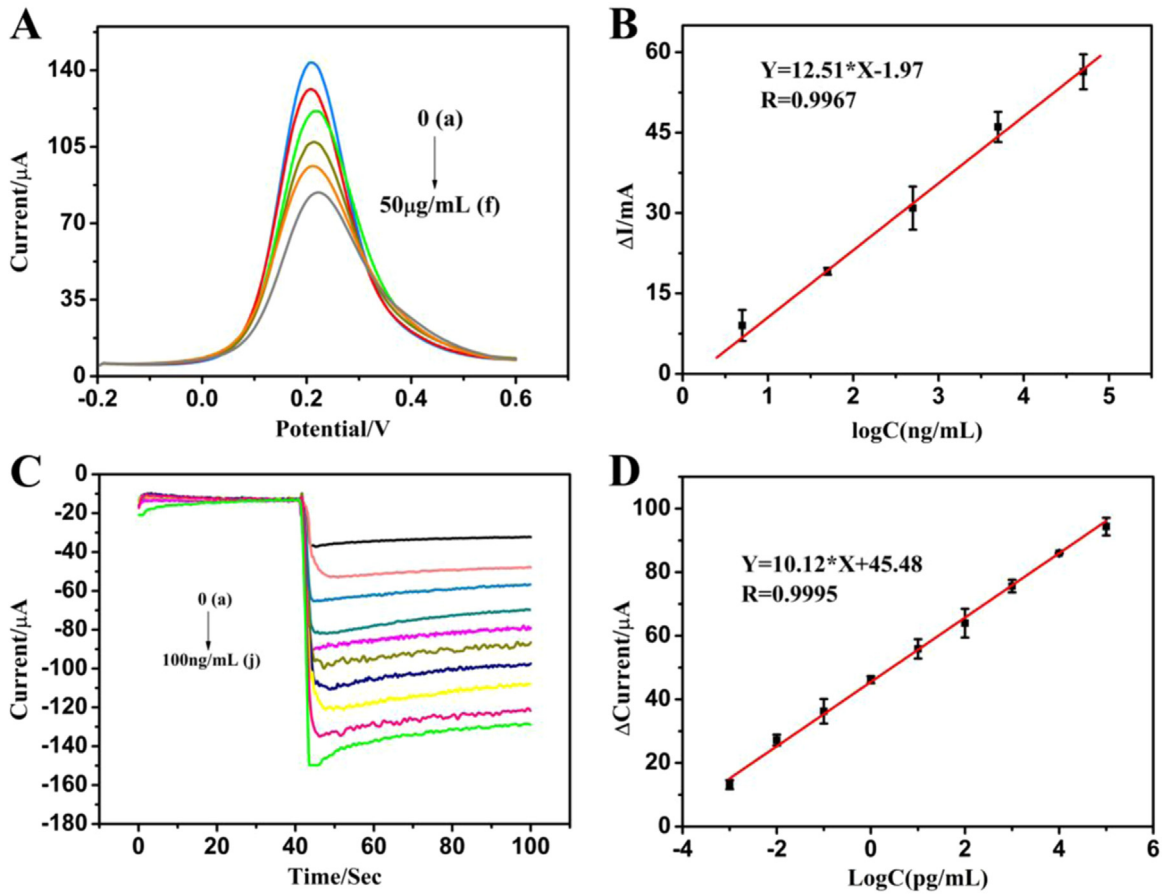

Fig. 4. (A): Differential pulse voltammetry responses of the proposed label-free biosensor for the determination of different concentrations of α2,6-sial-Gs: (a) 0 ng mL^{-1}; (b) 5 ng mL^{-1}; (c) 50 ng mL^{-1}; (d) 500 ng mL^{-1}; (e) 5 μg mL^{-1}; (f) 50 μg mL^{-1}. (B): The calibration curve of the label-free biosensor for different concentrations of α2,6-sial-Gs. (C) The amperometric i-t curves of the proposed biosensor with different target α2,6-sial-Gs concentrations in 5 mL of PBS (pH 7.0) with the addition of H_2O_2 (2.0 mol L^{-1}): (a) 0 fg mL^{-1}; (b) 1 fg mL^{-1}; (c) 10 fg mL^{-1}; (d) 100 fg mL^{-1}; (e) 1 pg mL^{-1}; (f) 10 pg mL^{-1}; (g) 100 pg mL^{-1}; (h) 1 ng mL^{-1}; (i) 10 ng mL^{-1}; (j) 100 ng mL^{-1}; (D) The calibration curve of the sandwich-type biosensor for different concentrations of α2,6-sial-Gs.

Table 1
Analytical performance compared with other methods of α2,6-sial-Gs detection.

Detection methods	Linear rage	Detection limit	Reference
Label-free biosensor	10 fg mL^{-1}- 1 μg mL^{-1}	0.003 pg mL^{-1}	(Li et al., 2015)
Label-free biosensor	0.1 pg mL^{-1}- 500 ng mL^{-1}	0.03 pg mL^{-1}	(Gao et al., 2014)
Dual-type responsive electrochemical biosensor	1 fg mL^{-1}- 5 μg mL^{-1}	0.69 fg mL^{-1}	**This work**

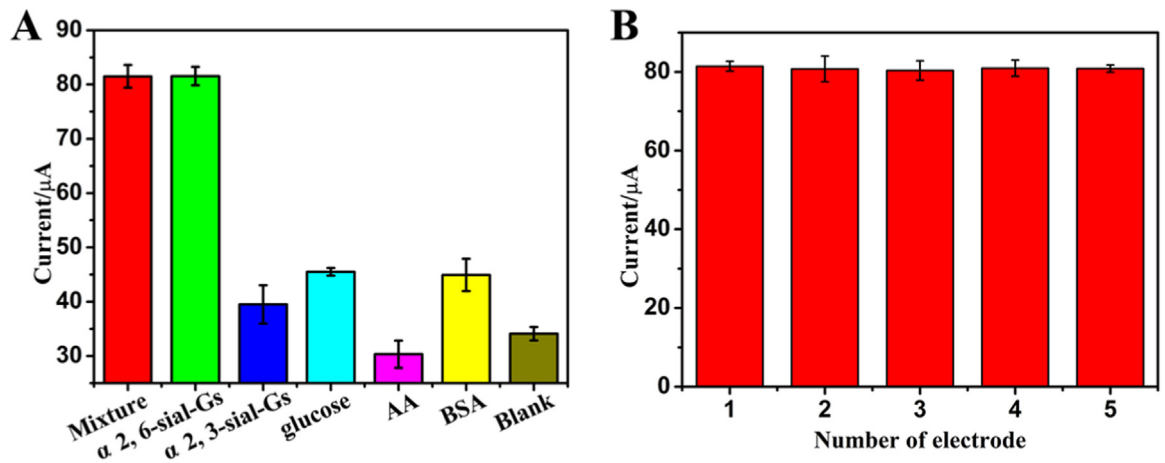

Fig. 5. (A) Specificity of the sandwich-type biosensor towards: 10 pg mL^{-1} of target, mixture, 1 ng mL^{-1} of α2,3-sial-Gs, 1 ng mL^{-1} of glucose, 1 ng mL^{-1} of BSA, and blank control; (B) Reproducibility of the sandwich-type biosensor fabricated on five different electrodes for the detection of 10 pg mL^{-1} of α2,6-sial-Gs.

which exhibited an ultrasensitive detection of α2,6-sial-Gs. This fabricated biosensor exhibited wide detection range, low detection limit, outstanding specificity, excellent reproducibility and stability. This method showed a potential for α2,6-sial-Gs determination in actual samples and could be expanded readily for detection of other glycoproteins in clinical practice. However, due to the biosensor fabrication requiring multiple modifications step, the biosensor was limited in practical application. Therefore, future work will be focused on developing a method for simplifying the preparation process, such as using codeposition and other novel nanotechnologies.

Credit author statement

Author declaration

We confirm that we have given due consideration to the protection of intellectual property associated with this work and that there are no impediments to publication, including the timing of publication, with respect to intellectual property. In so doing we confirm that we have followed the regulations of our institutions concerning intellectual property.

We further confirm that any aspect of the work covered in this manuscript that has involved either experimental animals or human patients has been conducted with the ethical approval of all relevant bodies and that such approvals are acknowledged within the manuscript.

Declaration of interest statement

Author declaration

We declare that we do not have any commercial or associative interest that represents a conflict of interest in connection with the work submitted.

We confirm that the manuscript has been read and approved by all named authors and that there are no other persons who satisfied the criteria for authorship but are not listed. We further confirm that the order of authors listed in the manuscript has been approved by all of us.

We understand that the Corresponding Author is the sole contact for the Editorial process (including Editorial Manager and direct communications with the office). He/she is responsible for communicating with the other authors about progress, submissions of revisions and final approval of proofs. We confirm that we have provided a current, correct email address which is accessible by the Corresponding Author and which has been configured to accept email from yucpaper@126.com.

Acknowledgements

We are grateful for the financial support from the National Natural Science Foundation of China (No. 81370403), Chongqing foundation and advanced research project (No. CSTC2015jcyjBX0053), Chongqing precision medical key technology research and development and demonstration projects (cstc2016shms-ztzx0042) and Chongqing Medical University scientific research cultivating fund (No. 201414).

Appendix A. Supporting information

Supplementary data associated with this article can be found in the online version at https://doi.org/10.1016/j.bios.2019.01.054.

References

Bemana, H., Rashid-Nadimi, S., 2017. Electrochim. Acta 229, 396–403.
Dall'Olio, F., Malagolini, N., diStefano, G., Minni, F., Marrano, D., Serafini-Cessi, F., 1989. Int. J. Cancer 44, 434–439.
Dong, X.Y., Mi, X.N., Zhang, L., Liang, T.M., Xu, J.J., Chen, H.Y., 2012. Biosens. Bioelectron. 38, 337–341.
Gao, L., He, J., Xu, W., Zhang, J., Hui, J., Guo, Y., Li, W., Yu, C., 2014. Biosens. Bioelectron. 62, 79–83.
Gessner, P., Riedl, S., Quentmaier, A., Kemmner, W., 1993. Cancer Lett. 75, 143–149.
Gevaerd, A., Blaskievicz, S.F., Zarbin, A.J.G., Orth, E.S., Bergamini, M.F., Marcolino-Junior, L.H., 2018. Biosens. Bioelectron. 112, 108–113.
Kim, S., Oh, D.B., Kang, H.A., Kwon, O., 2011. Appl. Microbiol. Biotechnol. 91, 1–15.
Harduin-Lepers, A., Vallejo-Ruiz, V., Krzewinski-Recchi, M.A., Samyn-Petit, B., Julien, S., Delannoy, P., 2001. Biochimie 83, 727–737.
Harvey, D.J., 2011. J. Chromatogr. B Anal. Technol. Biomed. Life Sci. 879, 1196–1225.
Li, Q., Yu, C., Gao, R., Xia, C., Yuan, G., Li, Y., Zhao, Y., Chen, Q., He, J., 2016a. Biosens. Bioelectron. 80, 674–681.
Li, Y., He, J., Niu, Y., Yu, C., 2015. Biosens. Bioelectron. 74, 953–959.
Li, Z., Miao, X., Xing, K., Peng, X., Zhu, A., Ling, L., 2016b. Biosens. Bioelectron. 80, 339–343.
Lima, H.R.S., da Silva, J.S., de Oliveira Farias, E.A., Teixeira, P.R.S., Eiras, C., Nunes, L.C.C., 2018. Biosens. Bioelectron. 108, 27–37.
Liu, Y., Wang, H., Xiong, C., Chai, Y., Yuan, R., 2017. Biosens. Bioelectron. 87, 779–785.
Nandan, R., Nanda, K.K., 2013. Nanoscale 00, 1–3.
Narang, J., Malhotra, N., Singh, G., Pundir, C.S., 2015. Biosens. Bioelectron. 66, 332–337.
Otsuka, H., Uchimura, E., Koshino, H., Okano, T., Kataoka, K., 2003. J. Am. Chem. Soc. 125, 3493–3502.
Park, J.J., Yi, J.Y., Jin, Y.B., Lee, Y.J., Lee, J.S., Lee, Y.S., Ko, Y.G., Lee, M., 2012. Biochem. Pharmacol. 83, 849–857.
Patil, S.A., Bshara, W., Morrison, C., Chandrasekaran, E.V., Matta, K.L., Neelamegham, S., 2014. Glycoconj. J. 31, 509–521.
Ribeiro, J.A., Pereira, C.M., Silva, A.F., Sales, M.G.F., 2018. Biosens. Bioelectron. 109, 246–254.
Saarinen, J., Welgus, H.G., Flizar, C.A., Kalkkinen, N., Helin, J., 1999. Eur. J. Biochem. 259, 829–840.
Sanzò, G., Taurino, I., Puppo, F., Antiochia, R., Gorton, L., Favero, G., Mazzei, F., Carrara, S., De Micheli, G., 2017. Methods 129, 89–95.
Schultz, M.J., Swindall, A.F., Wright, J.W., Sztul, E.S., Landen, C.N., Bellis, S.L., 2013. J. Ovarian Res. 6, 25.
Skrabalak, S.E., Chen, J., Au, L., Lu, X., Li, X., Xia, Y., 2007. Adv. Mater. 19, 3177–3184.
Wang, H.F., Ma, R.N., Sun, F., Jia, L.P., Zhang, W., Shang, L., Xue, Q.W., Jia, W.L., Wang, H.S., 2018. Biosens. Bioelectron. 122, 224–230.
Wang, Y., Ma, H., Wang, X., Pang, X., Wu, D., Du, B., Wei, Q., 2015. Biosens. Bioelectron. 74, 59–65.
Won, Y.H., Huh, K., Stanciu, L.A., 2011. Biosens. Bioelectron. 26, 4514–4519.
Wu, J., Chen, Y., Yang, M., Wang, Y., Zhang, C., Yang, M., Sun, J., Xie, M., Jiang, X., 2017. Anal. Chim. Acta 982, 138–147.
Yavas, O., Acimovic, S.S., Garcia-Guirado, J., Berthelot, J., Dobosz, P., Sanz, V., Quidant, R., 2018. ACS Sens. 3, 1376–1384.
Yang, F., Han, J., Zhuo, Y., Yang, Z., Chai, Y., Yuan, R., 2014. Biosens. Bioelectron. 55, 360–365.
Yuan, Q., He, J., Niu, Y., Chen, J., Zhao, Y., Zhang, Y., Yu, C., 2018. Biosens. Bioelectron. 102, 321–327.
Zhang, C., He, J., Zhang, Y., Chen, J., Zhao, Y., Niu, Y., Yu, C., 2018a. Biosens. Bioelectron. 102, 94–100.
Zhang, T., Chai, H., Meng, F., Guo, Z., Jiang, Y., Miao, P., 2018b. ACS Appl. Mater. Interfaces 10, 36796–36804.
Zhang, Y., Huang, Z., Wang, L., Wang, C., Zhang, C., Wiese, T., Wang, G., Riley, K., Wang, Z., 2018a. Anal. Chem. 90, 4733–4740.
Zhang, Y., Xia, J., Zhang, F., Wang, Z., Liu, Q., 2018b. Biosens. Bioelectron. 120, 15–21.
Zhao, Y., Wei, A., Zhang, H., Chen, X., Wang, L., Zhang, H., Yu, X., Yuan, Q., Zhang, J., Wang, S., 2017. Oncogenesis 6, e343.